Dissociation of 1,1,1-Trifluoroethane Behind Reflected Shock Waves: Shock Tube/Time-of-Flight Mass Spectrometry Experiments

Binod R. Giri and Robert S. Tranter*

Argonne National Laboratory, 9700 South Cass Avenue, Argonne, Illinois 60439

Received: September 22, 2006; In Final Form: January 5, 2007

The dissociation of 1,1,1,-trifluoroethane, a potential non-RRKM reaction, has been studied at 600 and 1200 Torr and high temperatures (1500−1840 K) using a new shock tube/time-of-flight mass spectrometer (ST/TOF-MS). These data obtained by an independent method are in good agreement with the laser schlieren, LS, experiments of Kiefer et al. [*J. Phys. Chem. A* **2004**, *108*, 2443−2450] and extend the range of that experimental dataset. The data have been simulated by both standard RRKM calculations and the non-RRKM model reported by Kiefer et al. but with $<\Delta E_{down}> = 750$ cm^{-1}. Both the RRKM and non-RRKM calculations provide equally good fits to the ST/TOF-MS data. Neither model simulates the combined ST/TOF-MS and LS datasets particularly well. However, the non-RRKM model predicts a pressure dependency closer to that observed in the experiments than the RRKM model.

Introduction

The thermal dissociation of 1,1,1-trifluoroethane, TFE, proceeds almost entirely via a four-center transition state eliminating HF and forming 1,1,-difluoroethene, DFE.

$$C_2H_3F_3 \rightarrow C_2H_2F_2 + HF \quad (1)$$

The simplicity of reaction 1 creates an almost ideal chemical thermometer that has been used with the single-pulse shock tube technique.[1,2] Consequently, the high-pressure limit rate coefficient, k_∞, has been determined several times both experimentally and theoretically, and the literature data are in excellent agreement.[2−8] The experimental determinations of k_∞ cover the temperature range 800−1320 K. Kiefer et al.[4] calculated k_∞ from 830 to 2500 K using conventional transition-state theory with the molecular and transition-state properties obtained from G3[9] calculations. The results of these calculations are in excellent agreement with the lower temperature experimental data.

Recent experiments on the decomposition of TFE by Kiefer et al.,[4] behind incident shock waves at low pressures using laser schlieren densitometry, LS, have shown a strong falloff from k_∞. However, even over the broad pressure range of the experiments, 15−550 Torr, surprisingly little pressure dependence in the measured rate coefficients was observed. This unusual behavior rendered simulation of the experimental data by a standard RRKM model impossible. Consequently, the authors proposed a simple modified RRKM model including slow intramolecular vibrational relaxation, IVR, suggesting that TFE dissociation may be non-RRKM in nature. With this model Kiefer et al. were able to simulate the LS experimental data reasonably well.

Barker and co-workers[10,11] subsequently tackled the notion of non-RRKM behavior in TFE dissociation with a number of theoretical methods and concluded that on the basis of the extant experimental data it cannot be determined if reaction 1 is RRKM or non-RRKM in nature. In particular, Stimac and Barker[11] demonstrated by classical trajectory calculations that IVR is likely to be too fast to affect the measurements of Kiefer et al. Consequently, if reaction 1 is truly non-RRKM, then a different explanation to that tentatively advanced by Kiefer et al. must be sought. Furthermore, Barker et al.[10] suggested that there may be systematic errors in the LS data that were not accounted for, indicating that additional experimental information on TFE dissociation at relatively low pressures and high temperatures is needed.

The LS data from Kiefer at al. are the only experimental results in the high-temperature falloff region for reaction 1. Cadman et al.[12] reported results for TFE dissociation at 1590−1865 K and 800 Torr that do lie considerably lower than the high-pressure limit but are only slightly lower than the so-called 'false high-pressure limit' calculated from Kiefer et al.'s non-RRKM model.[4] However, the data of Cadman et al. have been re-evaluated by Tsang,[13] who demonstrated that there may have been flaws in the original interpretation of the data. Consequently, the data from Cadman et al. must be considered with some caution.

The current work seeks to extend the experimental data on reaction 1 in the falloff region using an independent technique and a newly developed apparatus. The temperature and pressures of the falloff region in TFE decomposition are most accessible with a shock tube. However, unlike the previous experiments which were conducted behind incident shock waves with laser schlieren densitometry, the current work used reflected shock waves with time-of-flight mass spectrometry, TOF-MS, as the detection method. Thus, the experimental data from the current work is obtained by a completely different method than the earlier work of Kiefer et al., and the agreement or disagreement between the datasets should highlight the degree that systematic errors affect the LS and TOF-MS data as well as extending the experimental range for this unusual reaction.

Experimental Methods

A new shock tube/TOF-MS, ST/TOF-MS, apparatus has been constructed. The ST/TOF-MS, in particular the sampling

* To whom correspondence should be addressed. E-mail: tranter@anl.gov.

10.1021/jp066232n CCC: $37.00
Published on Web 02/13/2007

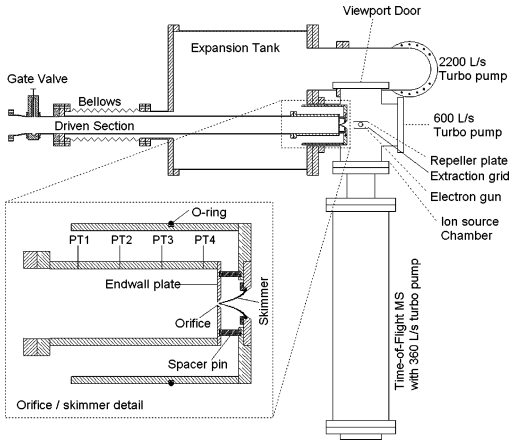

Figure 1. Schematic of the ST/TOF-MS interface. The inset shows the end of the shock tube and the nozzle/skimmer arrangement in detail. PT1−PT4 are the sidewall PCB 132A35 pressure transducers. For clarity, the end wall pressure transducer PT5 is not shown. The electron gun, not shown, is located on the top of the ion source chamber pointing into the page.

interface that couples the shock tube and TOF-MS, is described in detail elsewhere.[14] In order to test the new apparatus the thermal decomposition of cyclohexene, for which there is extensive data that are in good agreement, has been studied. The results of these initial experiments are reported in ref 14, and in particular, they show good accord with the high-temperature LS data from Kiefer et al.[15] at similar reaction conditions. A reasonably comprehensive description highlighting the operation of the new ST/TOF-MS follows in this paper. The apparatus consists of a shock tube connected via a differentially pumped nozzle/skimmer interface to a TOF-MS. The mass spectrometer is positioned orthogonal to the long axis of the shock tube as shown in Figure 1. This configuration is similar to that used by Krizancic et al.[16] but differs somewhat from that of Kern.[17] A comparison of the different configurations is made in ref 14.

The shock tube consists of a short, wide driver section (78 cm by 20 cm i.d.) separated from a driven section (7.3 m long) by an aluminum diaphragm. A number of ports are located on the driver section and provide connections to the gas supply, pump (Welch 1376 with foreline trap), and a pressure gauge (Sensotec SC-500). The pump is used both to evacuate the driver section, $\approx 10^{-3}$ Torr, in preparation for filling and to rapidly evacuate the shock tube at the end of an experiment. To facilitate this, the pump is connected to the driver section by a wide bore, solenoid-actuated, ball valve that can be remotely operated.

The first 6 m of the driven section following the diaphragm have an i.d. of 7.1 cm. A set of six pressure transducers (Dynasens CA-1135) is centered around a pair of windows (quartz, 6 mm thick, 27 mm width) located at ≈5 m. These are intended for LS experiments behind incident shock waves. Downstream of the windows a T-piece provides a connection via a high-vacuum valve to the mixing rig, pressure gauges (Leybold Ceravac), and pumps (Leybold 150 L/s turbo pump backed by a Leybold D16B oil pump with fore-line trap) for evacuation of the driven section and mixing rig. The driven section is filled and evacuated, $\approx 10^{-5}$ Torr, through this T-piece, and the pressure gauges are used to measure the loading pressure, P_1. Immediately after the T-piece a smooth, conical reducer changes the i.d. of the driven section to 6.1 cm to allow it to pass through a bellows into a large tank that forms the expansion chamber of the differentially pumped nozzle/skimmer interface, see Figure 1. The TOF-MS, interface, pumps, and hardware are all mounted on a frame with 3-axes adjustment. The bellows provides some flexibility in aligning the TOF-MS apparatus with the shock tube. More importantly, the separation between the ion source and sampling system can be altered while the apparatus is under vacuum to attain the best performance from the mass spectrometer, and this separation can be observed through a viewport, see Figure 1. A gate valve separates the narrower bore tube from the reducer and is used to isolate the TOF-MS interface while changing diaphragms.

During an experiment the driver section is filled with helium to a pressure P_4 and the driven section with the reagent mixture to a pressure P_1. By varying P_4/P_1 different reaction conditions, P_5, and T_5, behind the reflected shock waves may be obtained. Typically P_4 is fixed for one chosen P_5, e.g., 600 Torr, and P_1 varied to obtain a wide range of T_5 over a small range of P_5 as is usual in shock tube experiments. To fire the shock tube a four-bladed, sharp-tipped knife mounted on a shaft inside the driver section is manually driven into the diaphragm. The knife punctures and cuts the diaphragm so that it opens fully without breaking off fragments that could damage or block the sampling orifice located in the end wall of the driven section. Use of a diaphragm breaker allows P_4 and P_1 to be set accurately, giving reasonable control over the postshock conditions generated. In the current work experiments were performed at two nominal P_5, 600 and 1200 Torr. For the lower pressure experiments 0.004 in. thick aluminum diaphragms were used and 0.008 in. aluminum diaphragms for the 1200 Torr experiments.

P_5 and T_5 are obtained in the normal manner from the standard shock wave equations[18] using T_1, P_1, and the measured incident shock wave velocity. The reduction in diameter in the driven section causes a small acceleration of the incident shock wave. Thus, in the ST/TOF-MS experiments the incident shock velocity is measured downstream of the reducer close to the end wall of the driven section. To obtain the shock wave velocity at this location a set of miniature piezoelectric pressure transducers (PCB 132A35, identified in Figure 1 as PT1 to PT4) was installed in the side wall of the driven section inside the expansion tank. The transducers are spaced 76.2 mm apart with PT4 located 27 mm from the end wall. A fifth pressure transducer, PT5, is located in the end wall parallel to the shock tube. The passage of the incident shock wave over the pressure transducers is used to trip timer circuits that are accurate to 0.1 μs, and by measuring the time taken for the shock wave to travel the known distance between pressure transducers the shock velocity is obtained. Little attenuation of the shock wave was observed in this work.

The end wall of the driven section closes the shock tube and also forms the entrance to the TOF-MS interface; see inset in Figure 1. In these experiments a flat stainless steel plate, 3.2 mm thick, with a centered hole of 0.4 mm i.d. formed the end wall. The back of the plate was counter-bored into a cone centered on the orifice, leaving a wall thickness of about 0.5 mm at its entrance. Gases from the shock tube flow continuously through the orifice and into the large expansion chamber, evacuated by a 2200 L/s turbo pump, which after loading the driven section of the shock tube retains a pressure of $<10^{-4}$ Torr. The rapid expansion of the gas jet from the orifice freezes the composition of the mixture at the high-temperature composition sampled from the shock tube.[14] An axisymmetric skimmer (Beam Dynamics Inc. model 2) is aligned with the nozzle, and the tip of this skimmer is about 3 mm from the orifice in the end wall. Separation and alignment between the nozzle and skimmer are maintained with brass

spacer pins, as shown in Figure 1. For these TOF-MS experiments skimmers with two different openings, 0.48 and 0.32 mm, were used. The smaller skimmer reduced the load on the TOF-MS pumps but also reduced the signal intensities from the mass spectrometer; however, no difference in the kinetic data obtained was discernible.

The use of the nozzle/skimmer arrangement instead of the simple nozzle used by Kern[17] minimizes one of the thornier problems associated with sampling gases from behind reflected shock waves through the driven section end wall. That is the effect of co-sampling the cooler gases from the end wall thermal boundary layer with the shock heated gases. This problem has been analyzed in detail[14,19−21] and for the current configuration, where a core sample of the jet of gas expanding through the large end wall orifice is taken by the skimmer; at least several milliseconds are required for the thermal boundary layer to grow sufficiently to contaminate the gases entering the TOF-MS. A maximum of 2 ms of data behind the reflected shock wave is captured in these experiments, and it is only the first 100−200 μs that really yield information about the initial rate of reaction. Consequently, the thermal boundary layer is unlikely to cause problems in this work. A detailed discussion of the sampling from this apparatus is available in ref 14 along with a comparison of the use of a small, conical nozzle without a skimmer as used in earlier instruments[17,20] in place of the nozzle/skimmer interface used here and by Krizancic et al.[16]

The shock tube/TOF-MS interface is formed by the orifice, expansion tank, and skimmer. The gases that pass through the skimmer enter a six-way cross, the ion source chamber, Figure 1. A 600 L/s turbo pump is mounted directly opposite the skimmer and exhausts the molecular beam from the ion source. The TOF-MS is mounted orthogonal to the shock tube, and the ion optics of the TOF-MS extend into the ion source chamber. The repeller plate and extraction grid, Figure 1, along with an electron gun form the actual ion source which is centered in the six-way cross. The electron gun is mounted on the cross so that the emitted electron beam passes between the repeller plate and extraction grid perpendicular to the molecular beam from the skimmer. As the molecular beam traverses the ion source a small fraction of the species in the molecular beam is ionized. The positive ions are then extracted via the ion optics into the drift/flight tube of the TOF-MS for mass separation and detection with a multichannel plate detector, the MCP. In these experiments a range of ionizing electron energies from 28 to 34 eV was used. These electron energies are sufficient to generate well-defined mass spectra for easily ionized species, e.g., organic species, argon, krypton, etc., but minimize the ionization of the bath gas neon which has a relatively high ionization energy, 21.5 eV. This reduces the opportunity for Ne^+ ions to saturate the MCP.

The TOF-MS is a R. M. Jordan reflectron and is operated in reflectron mode to take advantage of the superior focusing obtained as compared to the linear mode. In this instrument packets of ions are generated by deflecting the electron beam, so that it moves in and out of the space between the repeller and extraction grid. When the electron beam moves out of the ion source the voltage on the extraction grid is lowered relative to the repeller and the positive ions are extracted and accelerated into the drift region of the TOF-MS where the ions are separated by their mass/charge ratio, m/z. As all ions experience the same accelerating voltage the ions with smaller m/z reach a higher velocity than the ions with larger m/z and arrive at the MCP earlier. The time from the initial extraction to the arrival at the detector is measured for each m/z. This flight time can be converted to m/z by the following equation[22]

$$m/z = a(t_f)^2 + b \quad (2)$$

where a and b are constants determined by measuring the flight time for known m/z for a particular configuration of the TOF-MS. Here t_f is the time taken between the ions having been extracted from the ion source and arriving at the MCP.

After a period that is long enough for all the ions from an injection pulse to arrive at the detector the extraction grid is set to the same voltage as the repeller and the electron beam is focused back into the space between them, generating a new ion packet. In this way mass spectra are obtained at known time intervals with the deflection of the electron beam and voltage changes on the extractor grid controlled via a signal generator.

One modification has been made to the R. M. Jordan TOF-MS: the flight tube has been shortened to 381 mm to reduce t_f, thereby permitting the analysis cycle rate to be increased without successive spectra becoming intermingled. An analysis cycle is defined as the generation of ions in the ion source, extraction into the TOF-MS, and detection by the MCP. The higher analysis cycle rate permits the molecular beam eluting from the shock tube to be sampled more frequently, leading to more accurate measurement of the time-dependent concentration profiles in the molecular beam. The price to pay for a shorter flight tube is that the mass spectral resolution is decreased for large m/z. In the current work baseline separation is retained for species differing by 1 amu and the reduced resolution at high m/z is of no concern.

The output of the MCP is an analog signal which is captured using an Acqiris DP210 single-channel digitizer operating at 1 or 2 GS/s (1 or 0.5 ns per data point). Simultaneously, the voltage pulses that control the generation and injection of ions are captured using an Acqiris DP306 single-channel digitizer operating at 100 MS/s. The two digitizers are synchronized by a single trigger pulse that is generated by the passage of the incident shock wave over PT1 of Figure 1. Data are acquired continuously for up to 2 ms and include both preshock and postshock spectra. If the ionization source is pulsed at a sufficiently high frequency then the mass spectra from successive ionization events can be interwoven in the data files. If light ions from one ionization event overtake the heavier, slower moving ions from a prior ionization event then 'ghost' peaks appear in the mass spectra for the individual time periods that clearly do not belong to the same analysis cycle. Using in-house software the data acquired from the MCP can be split into the time segments corresponding to each ionization event and deconvoluted. This technique allows the ion source to be pulsed at a higher rate than would be apparent from the flight time of the heaviest ions, improving the time resolution of the experiments. However, care must be taken to ensure that ions from different cycles do not strike the MCP simultaneously and that baseline resolution between the peaks is maintained.

Shock tube experiments are inherently single shot with some variation occurring in the postshock conditions from one experiment to the next even in the most carefully designed and operated apparatus. Furthermore, during an experiment the species concentrations change extremely rapidly. The combination of these two facts renders signal averaging to improve signal/noise impossible in ST/TOF-MS experiments. Thus, relatively high reagent concentrations are needed to produce strong peaks in the mass spectra and an internal standard is added to the reagent mixtures. This internal standard helps calibrate the fluctuations in signal intensities that occur, even

in nonreacting mixtures, due to the subtle differences in each ionization event and the increases in ion signals due to increasing pressure in the ion source chamber that occur in a shock wave experiment.[16,17]

The sequence of events in a shock wave experiment following diaphragm rupture is then as follows: First, the incident shock wave arrives at the first PCB pressure transducer, PT1, and triggers the pulsing of the ion source and the two data acquisition boards; this also starts the timers that are used to calculate shock velocity from the measured time for the incident shock wave to travel between transducers. After 1 or 2 ms data acquisition stops and solenoid valves are opened to vent the shock tube through the high-speed oil pump on the driver section. The power to the TOF-MS is turned off to prevent arcing in the ion source due to the high pressures in the ion source chamber that are attained several tens of milliseconds after the reflected shock wave is formed.

During the course of this work the shock tube and TOF-MS were periodically cleaned to remove soot deposits. No discernible difference in the measured rate coefficients obtained from the shock tube after it was cleaned or just prior to cleaning was observed. However, excessive soot deposits did tend to partially block the sampling nozzle, reducing the mass flow into the TOF-MS and hence reducing the measured peak areas.

Reagent Mixtures. Reaction mixtures were prepared in a glass vessel (50 L) and allowed to stand overnight before use. Typically 200 Torr total pressure of reagent mixture was prepared, permitting 15−30 experiments to be performed with the same mixture. Approximately one-half of the experiments were performed with a mix of 4% 1,1,1-trifluoroethane (Synquest 99.9%), 4% argon (Linde 99.999%), and the balance neon (Linde 99.999%) which is suitable for use with the 0.32 mm skimmer. More dilute mixtures of 2% and 2.5% TFE and 2% and 2.5% argon were used with the 0.48 mm skimmer. All chemicals were used as supplied without further purification. The major impurities in the TFE are 1,1-difluoroethene and hydrogen fluoride, which arise from the manufacturing process. Argon acts as an internal standard with the concentration selected to give a peak area in the mass spectrum similar to that of the reagent.

Results and Discussion

Experiments were mainly performed at two nominal postshock pressures, P_5, of 600 and 1200 Torr, and $T_5 = 1500-1840$ K; the exact conditions for each experiment are given in the Supporting Information. These conditions encompass and extend the range of the literature data in the falloff region.[4,12] Attempts were made to obtain kinetic data at lower pressures than 600 Torr; however, with the current configuration of the ST/TOF-MS interface such lower pressure experiments are difficult and prone to excessive scatter in the extracted concentration vs time profiles and thus were not further pursued.

A sample profile ($P_5 = 590$ Torr, $T_5 = 1707$ K) is shown in Figure 2, where the downward spikes are the mass spectra and the upward pulses are the timing signals used to generate ions in the ion source and then inject them into the TOF-MS. Each segment between the timing spikes represents injection of one ion packet, and the abscissa shows the time after the TOF-MS was triggered by the incident shock wave passing PT1. Injection of the ion packets occurs on the falling edge of the timing signal, and the time between the rising and falling edges represents the ionization period, typically 0.4 μs, during which electrons are injected into the ion source. The end of one injection pulse and start of the next can be seen in Figure 3.

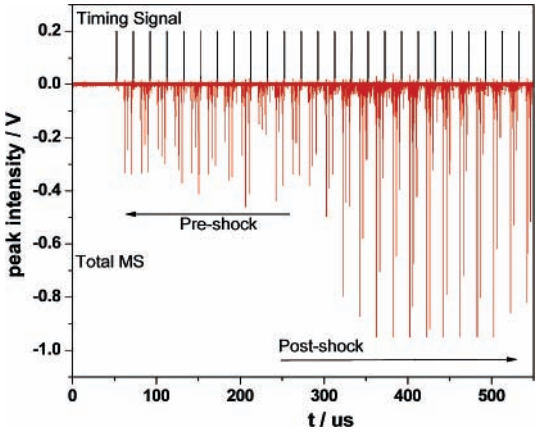

Figure 2. Example of raw data obtained from a ST/TOF-MS experiment. The red downward line, labeled Total MS, shows the data from the TOF-MS MCP detector recorded on the Acqiris DP210 board. The black line shows the ion source timing signals recorded on the Acqiris DP306 board. The ion source was pulsed at 50 kHz, and a total of 1000 μs signal was recorded (truncated here). Postshock conditions are $P_5 = 590$ Torr and $T_5 = 1707$ K. See text for a description of the increase in peak sizes after 250 μs.

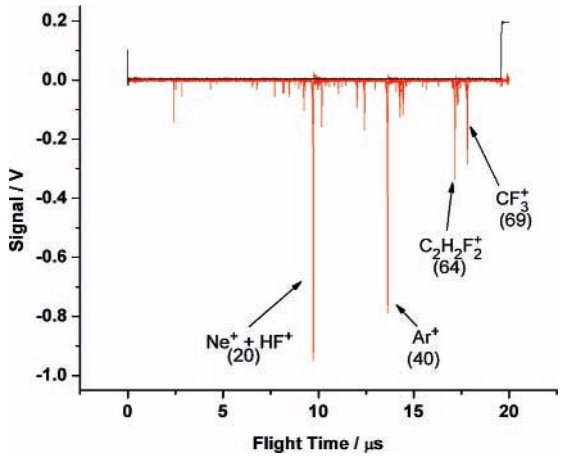

Figure 3. Single time segment showing reaction extracted from Figure 2. The flight times are relative to the injection pulse for this segment, the end of which is seen on the left side of the upper, black line. Postshock conditions are $P_5 = 590$ Torr and $T_5 = 1707$ K; ion source pulsed at 50 kHz. The numbers in parentheses denote m/z for the ions; obtained by calibration.

The early part of the data in Figure 2, up to about 250 μs, represents data acquired before the incident shock wave reflects from the orifice plate at the end of the driven section. The remainder of the figure represents the post-reflected shock part of the experiment. The steady rise in the apparent peak heights after ≈250 μs is due to the slowly increasing pressure in the ion source which lags behind the step change in pressure that occurs in the shock tube behind the shock wave. This is an effect that is commonly seen in ST/TOF-MS work.[14,16,17,19,20] To compensate for the increase in signal due to changing conditions in the ion source, which affects all species equally, all peak areas are scaled by the argon peak area for the appropriate time segment.[14,16,17]

The raw data from Figure 2 are split into the individual time periods and a mass spectrum for each time period obtained using in-house software; see Figure 3 which shows a single period from Figure 2. A time period is defined as the time from injection to a time greater than t_f for the heaviest ion injected. In these experiments 20 μs is used based on t_f for CF_3^+. A time period may be longer than the time between ionization pulses;

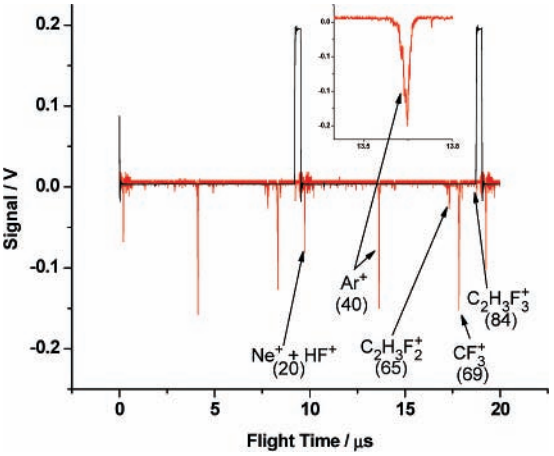

Figure 4. A 20 μs time segment from an experiment where T_5 is too low for reaction: $P_5 = 447$ Torr, $T_5 = 1390$ K. The ion source was pulsed at 105 kHz, and the timing signals are shown in the black (top) line. The flight times are relative to the injection pulse shown at the extreme left, and the two pulses at 9.5 and 19 μs are subsequent ionization events. The unlabeled peaks appearing at shorter times than 10 μs are from the heavy ions from the prior ionization event. The inset figure shows the shape of the Ar^+ peak. The numbers in parentheses denote m/z for the ions; obtained by calibration.

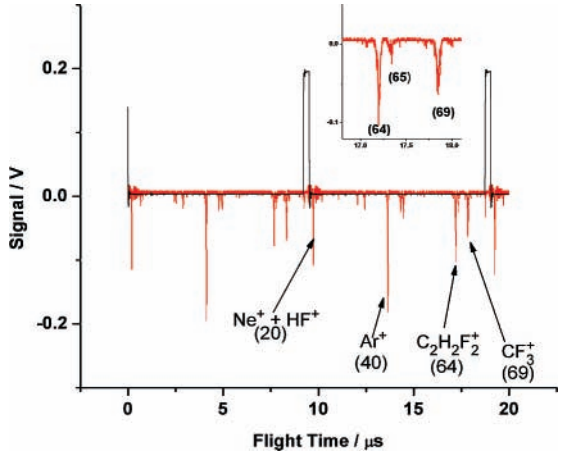

Figure 5. Single time segment from an experiment where reaction is occurring: $P_5 = 596$ Torr and $T_5 = 1732$ K. The ion source was pulsed at 105 kHz. The timing signals are shown by the black (top) line, and the red line represents the mass spectrum. Flight times of the ions are relative to the injection pulse for the time segment. The inset expands the peak shapes for the $C_2H_2F_2^+$ ion and the CF_3^+ ion. Note the small peak at $m/z = 65$ ($C_2H_3F_2^+$) which has baseline separation from the strong $m/z = 64$ peak. The numbers in parentheses denote m/z for the ions; obtained by calibration.

see Figure 4 for an example. The flight times of ions relative to the injection pulse are calculated and converted to m/z using eq 1. To determine the constants in eq 1 t_f was measured for Ne^+ and CF_3^+ ions.

The mass spectrum for a single time segment from an experiment where T_5 was too low for reaction is shown in Figure 4. It is clear that no peak appears at $m/z = 84$; the mass of TFE. However, a strong peak at $m/z = 69$ is observed and a peak at $m/z = 65$. The $m/z = 69$ peak is CF_3^+, and the $m/z = 65$ is $C_2H_3F_2^+$, both of which are formed from fragmentation of the parent molecule in the ion source and not from decomposition in the shock tube. The ratio of peak areas $C_2H_3F_2^+/CF_3^+$ is about 0.2. No peak at $m/z = 64$, $C_2H_2F_2^+$, the parent and strongest peak of DFE, is seen. These observations are consistent with the electron impact mass spectrum for TFE available from NIST.[23] The CF_3^+ ion is only formed from TFE fragmentation and thus used to represent TFE in interpreting the data.

Furthermore, as CF_3^+ is the heaviest ion it sets the frequency limit at which the ion source can be pulsed without intermingling ions from different events. Here, the flight time for CF_3^+ is about 17.6 μs, and a convenient pulsing rate is thus 50 kHz or once every 20 μs. Experiments were performed with the ion source pulsed at 50 and 105 kHz (9.52 μs) and similar results obtained. Example spectra are shown in Figures 3 and 5. At the higher repetition rate the spectra from successive ionization events begin to overlap but the time resolution of the experiment doubles and improves the accuracy of the data. A higher pulse rate of 105 kHz was used instead of 100 kHz to move the $m/z = 20$ peak away from some electrical noise that occurred on each ionization cycle.

The point in the dataset where the reflected shock wave occurs, t_0, can be located by two methods. In the first the time for the shock wave to travel from the triggering pressure transducer, normally PT1 in Figure 1, to the center of the ionization volume is calculated from $t_0 = t_1 + t_2$. Here t_1 is the measured time for the incident shock wave to travel from PT1 to PT5, the end wall pressure transducer. t_2 is the time taken for the gas to flow from the orifice to the center of the ionization volume, which is estimated from the jet properties.[14]

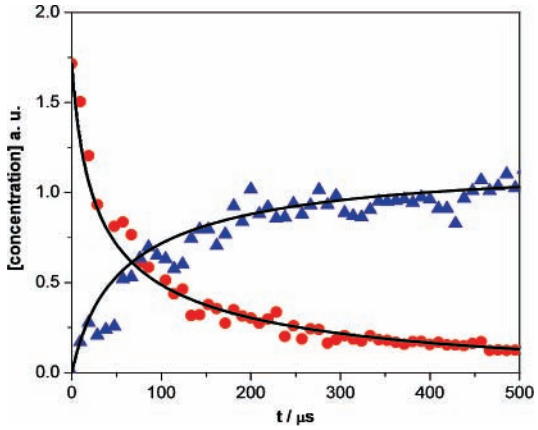

Figure 6. Plot of concentration vs time behind reflected shock wave for one experiment. $P_5 = 611$ Torr and $T_5 = 1803$ K: (red circle) 1,1,1-trifluoroethane and (blue triangle) 1,1-difluoroethene. Solid lines represent the model results. Each point represents one time segment behind the reflected shock wave.

In the second method the raw data signals of peak area against time are inspected and the time origin located at the point where the signals start to increase. This increase from the pressure rising in the ion source is brought on by the increase in pressure behind the reflected shock wave. Both methods lead to minor differences in the location of t_0, but good agreement between them is observed.

Once the peaks have been identified, the area of each peak of interest is scaled by the argon peak area[14,16,17] and concentration vs time profiles are obtained; see Figure 6 for an example. Rate coefficients are then extracted by locating t_0 and simulating the experimental data using the reaction mechanism shown in Table 1. The simulations have been conducted with a computer code designed for chemical kinetic simulations in incident and reflected shock waves which also accounts for nonisothermal effects (here $\Delta T \approx 10\%$ and $\Delta P \approx 10\%$) that arise due to the species concentrations and heats of reaction. The thermodynamic properties are entered into the code as set of six coefficients for each species based on an inverse T series.[24] All thermodynamic data were taken from the recent publication of Burcat et al.[25] In the simulation an initial estimate of the rate coefficient

TABLE 1: Reaction Mechanism Used To Simulate TFE Dissociation[a]

reaction	log *A*	n	E	source
1. $CH_3CF_3 \rightarrow CH_2CF_2 + HF$	44.51	−9.34	78.5	b
2. $C_2H_2F_2 \rightarrow CHCF + HF$	13.10	0.0	80.07	c

[a] Rate coefficients are given in the form $\log k\ (s^{-1}) = \log A + n \log T - E/2.303RT$, units in mol, kcal, and K. [b] Obtained from a fit to the LS and ST/TOF-MS data. This fit is applicable only over the range of the experimental data, $P = 100 - 1200$ Torr and $T = 1500 - 2400$ K. [c] See reference 26.

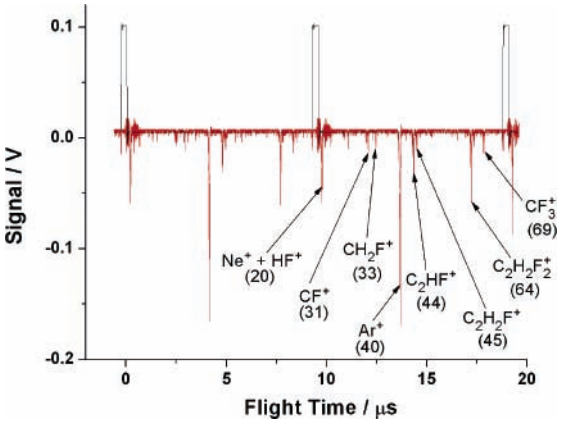

Figure 7. A 20 μs time segment taken after 180 μs of reaction time in an experiment where $P_5 = 1523$ Torr and $T_5 = 1823$ K; the ionization cycle was 105 kHz. The species distribution indicates that almost all the TFE has been consumed and that the only products are DFE and HF. The minor peaks are fragments from ionization of DFE. The peaks in the mass spectrum are identified, and the corresponding *m*/*z* values are given in parentheses. The black line shows the timing signal, and the red line represents the mass spectrum. The flight times are relative to the injection pulse shown at the extreme left, and the two pulses at 9.5 and 19 μs are subsequent ionization events.

for reaction 1 is made and then iteratively varied to obtain agreement with the experimental concentration/time profile.

The data in Figure 6 represent one of the highest temperature experiments performed in this work, and the simple two-reaction mechanism simulates the data very well. The simulations also predict that <5% of the DFE formed by reaction 1 is consumed by reaction 2 in the first 200 μs of reaction. Thus, it is apparent that even at the highest temperatures of this work reaction 2 plays only a minor role but is included for completeness. Furthermore, Figure 7 shows a mass spectrum taken 180 μs after t_0 from an experiment where $T_5 = 1823$ K and $P_5 = 1523$ Torr, where the minor peaks ($m/z = 45$, 44, 33, and 31) have been identified, and these are consistent with fragments from electron impact ionization of DFE.[23] The minor peaks are also observed in the mass spectra shown in Figures 3−5, which were obtained from much lower temperature experiments, and the relative ratios of $m/z = 45$, 44, 33, and 31 to $m/z = 64$, the parent DFE peak, do not vary significantly. The small amount of fluoroethyne, $m/z = 45$, formed in reaction 2 at high temperatures introduces an almost undetectable change in the $m/z = 45$ peak area and has no influence on the TFE decomposition rate. Thus, based on the mass spectral data and the good quality of the simulations it can be concluded that within the experimental observation time the simple mechanism in Table 1 is sufficient to describe the pyrolysis of TFE.

For TFE strong, unique peaks for both the parent and product ions are observed in the mass spectra which allow the loss of TFE and formation of DFE to be simulated with confidence. The second product HF has the same *m*/*z*, and hence flight time, as the bath gas neon and is thus not used in the interpretation

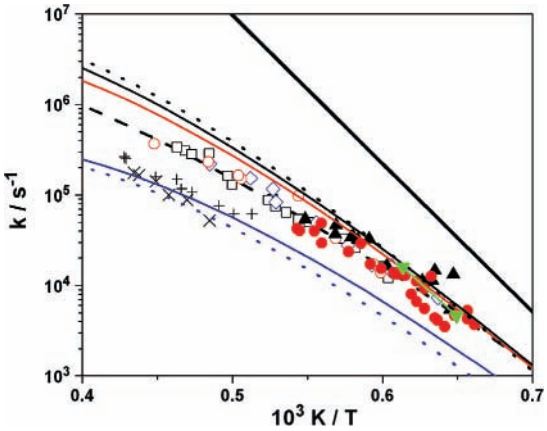

Figure 8. Comparison of TOF-MS data and LS experiments from Kiefer et al.[4] TOF-MS: (red solid circle) 600 Torr; (black solid triangle) 1200 Torr. LS: (black open square) 100 Torr, (blue open diamond) 350 Torr, (red open circle) 550 Torr, (+) 35 Torr, (×) 15 Torr. Cadman et al.[12] (Green inverted triangle) 800 Torr. (- - -) Non-Arrhenius fit to the 100−1200 Torr data, (heavy black line) theoretical k_∞ from Kiefer et al.[4] Non-RRKM calculations: (blue solid line) 35 Torr, (red solid line) 600 Torr, (black solid line) 1200 Torr. RRKM calculations: (blue dotted line) 35 Torr, (black dotted line) 1200 Torr.

of the experimental data as it cannot be distinguished from the neon signal. At low enough electron impact energies in the ion source the ionization of neon can be completely suppressed and in principle HF concentrations obtained. However, under these conditions the peaks for all the species are relatively weak and poorly formed, and as signal averaging cannot be used, the errors in an experiment increase. Thus, it is preferable to sacrifice the HF peak and obtain well-formed peaks for TFE and DFE.

The experimental data are tabulated in the Supporting Information, and the rate coefficients are also shown in Figure 8, where they are compared with the earlier LS experiments of Kiefer et al.[4] There is no discernible difference between the results of the ST/TOF-MS experiments using the different reagent mixtures, and the data are plotted using the same symbol for a particular pressure. At $T_5 \approx 1840$ K the extracted rate coefficients apparently no longer increase with increasing T_5. This effect is most likely from the reaction becoming too fast to monitor accurately with the time resolution of these experiments, and for this work experiments performed above 1840 K are not included in the data interpretation. The abrupt leveling off in extracted rate coefficients has also been observed in several other systems studied with this apparatus over different ranges of T_5 and is unlikely to be due to thermal boundary layer effects becoming more significant at high T_5.[14] With the current configuration of the apparatus we estimate that the largest rate coefficients that can be measured with confidence are in the range $4-7 \times 10^4$ s^{-1} with the exact value being system dependent. An error analysis has been conducted for the ST/TOF-MS experiments. The largest source of uncertainty in the calculated rate coefficients arises from the location of t_0. This is due to the fluctuations in peak areas from one ionization event to the next and the time resolution defined by the ionization cycle. An estimated error of 30% in the extracted rate coefficients is proposed.

Over the temperature range 1500 K < T < 1840 K the 600 and 1200 Torr the ST/TOF-MS data exhibit some scatter and based on best fit curves to each data set differ by 20−35% from each other. However, a statistical analysis based on the *F* value and *P* value indicates that the two datasets are statistically indistinguishable at the 95% confidence level, which implies that the two datasets could be treated as one with no pressure

dependence. The range of the ST/TOF-MS experiments overlaps the 100−550 Torr LS experiments of Kiefer et al.,[4] and there is good agreement between the rate coefficients obtained in the100−550 Torr LS data and the ST/TOF-MS results. Thus, the TOF-MS data extend the lower end of the experimental temperature range and show virtually no pressure dependence, which is in accord with the observation made by Kiefer et al.[4] in the pressure regime 100−550 Torr. Additionally, the ST/TOF-MS data provide support for the validity of the LS data as it is unlikely that two such different experimental techniques would be subject to similar systematic errors.

The original single-pulse shock tube data of Cadman et al.[12] which were reported for $T_5 = 1590-1865$ K and $P_5 \approx 800$ Torr are also shown in Figure 8. However, due to the aforementioned potential problems with these data we will not attach too much importance to them, but we note that they fit very well with the ST/TOF-MS data at a similar pressure.

In Figure 8 results are shown from calculations using the standard RRKM model and the non-RRKM, slow IVR, model taken from Kiefer et al. The LS experiments were performed in krypton, whereas the ST/TOF-MS experiments used neon as the bath gas. This difference is accounted for in both the standard and modified models by the Lennard−Jones parameters, and for neon ($\sigma = 2.82$ Å, $\epsilon/k_B = 32.8$ K) these were taken from Reid et al.,[27] with the other parameters being those reported by Kiefer et al. The change in using krypton or neon as the bath gas is negligible, as expected, and the results reported here are for neon. In these calculations $<\Delta E>_{down} = 750$ cm^{-1} instead of the 1000 cm^{-1} used by Kiefer et al., a minor modification. The smaller $<\Delta E>_{down}$ gave an improved fit to the ST/TOF-MS experiments and the higher temperature 100−550 Torr LS experiments while retaining a reasonable fit to the 35 Torr LS dataset, although the fit to the 35 Torr LS data is perhaps not as good as that reported by Kiefer et al. with $<\Delta E>_{down} = 1000$ cm^{-1}.

There appears to be little to distinguish the results of the RRKM and non-RRKM calculations shown in Figure 8. However, the results of the 35 Torr RRKM calculations are smaller those obtained from the 35 Torr non-RRKM calculations, but the 1200 Torr calculations show the reverse behavior with the RRKM results being larger than the non-RRKM results. This indicates that the non-RRKM model yields a smaller pressure dependency than the RRKM calculations, which is the trend shown by the complete experimental dataset. In the temperature region covered by the current work both the RRKM and non-RRKM calculations provide equally good fits to the ST/TOF-MS data. The RRKM calculations predict about a 30% difference between the rate coefficients for the 600 and 1200 Torr experiments, and the non-RRKM results predict approximately a 15% difference with the results of both calculations being slightly higher than the experimental results. However, when the calculations are extended to the higher end of the temperature range of the LS experiments it is clear that neither the RRKM or non-RRKM calculations simulate the high-temperature data particularly well, although the non-RRKM model does make some improvement.

In the ST/TOF-MS experiments that overlap with the LS experiments no evidence was found of secondary reactions generating free radicals which would tend to increase the apparent, measured rate coefficients for reaction 1. Consequently, considering the good agreement between the LS and ST/TOF-MS experiments and the abnormally small pressure dependency in the higher temperature data, the non-RRKM calculation appears to provide a better fit to the experimental data. However, based on the work of Barker et al.[10,11] it would appear that the notion of slow IVR, as encapsulated in the non-RRKM model, being responsible for the unusual pressure dependency of reaction 1 may be incorrect, and some other explanation for this behavior will be required.

Conclusions

The new ST/TOF-MS experiments behind reflected shock waves are in very good agreement with the earlier 100−550 Torr LS data from Kiefer et al.[4] The results of the current work were obtained using a completely different experimental technique to that of Kiefer et al., and it is extremely unlikely that systematic errors in both experiments would result in data in such good agreement. From the ST/TOF-MS and LS results for TFE decomposition it is apparent that neither the non-RRKM model nor the RRKM model of Kiefer et al. can adequately describe all the experimental data. Thus, although the new ST/TOF-MS data provide support for the LS experiments it is still undecided whether TFE decomposition is RRKM or non-RRKM at elevated temperatures. While the concept of slow IVR may not be the explanation for the observed pressure dependency in reaction 1, any model, RRKM or non-RRKM, must predict all the data, and currently only the modified RRKM model of Kiefer et al. comes close to doing this. It would be desirable to extend the range of the low-pressure experimental data as the small pressure dependency observed in the rate coefficients from 15 to 1200 Torr is a crucial feature of this unusual reaction.

Acknowledgment. The authors wish to thank J. H. Kiefer for many helpful discussions and his comments during this work and the preparation of the manuscript. This work was performed under the auspices of the U.S. Department of Energy, Office of Basic Energy Sciences, Division of Chemical Sciences, Geosciences, and Biosciences, under Contract No. W-31-109-Eng-38.

Supporting Information Available: Experimental data (T_5, P_5, and rate coefficient for reaction 1) are available in tabular form. This material is available free of charge via the Internet at http://pubs.acs.org.

References and Notes

(1) Tsang, W. In S*hock Tubes in Chemistry*; Lifshitz, A., Ed.; Marcel Dekker: New York, 1981.
(2) Tranter, R. S.; Sivaramakrishnan, R.; Srinivasan, N. K.; Brezinsky, K. *Int. J. Chem. Kinet.* **2001**, *33*, 722.
(3) Tsang, W.; Lifshitz, A. *Int. J. Chem. Kinet.* **1998**, *30*, 621.
(4) Kiefer, J. H.; Katopodis, C.; Santhanam, S.; Srinivasan, N. K.; Tranter, R. S. *J. Phys. Chem. A* **2004**, *108*, 2443.
(5) Tschuikow-Roux, E.; Quiring, W. J. *J. Phys. Chem.* **1971**, *75*, 295.
(6) Rodgers, A. S.; Ford, W. G. F. *Int. J. Chem. Kinet.* **1973**, *5*, 965.
(7) Mitin, P. V.; Barabanov, V. G.; Volkov, G. V. *Kinet. Catal.* **1988**, *29*, 1279.
(8) Sianesi, D.; Nelli, G.; Fontanelli, R. *Chim. Ind. (Milan)* **1968**, *50*, 619.
(9) Curtiss, L. A.; Ragavachari, K.; Redfern, P. C.; Rassolov, V.; Pople, J. A. *J. Phys. Chem. A* **1998**, *109*, 7764.
(10) Barker, J. R.; Stimac, P. J.; King, K. D.; Leitner, D. M. *J. Phys. Chem. A* **2006**, *110*, 2944.
(11) Stimac, P. J.; Barker, J. R. *J. Phys. Chem. A* **2006**, *110*, 6851.
(12) Cadman, P.; Day, M.; Trotman-Dickenson, A. F. *J. Chem. Soc. (A)* **1971**, 1356.
(13) Tsang, W. *Int. J. Chem. Kinet.* **1973**, *5*, 643.
(14) Tranter, R. S.; Giri, B. R.; Kiefer, J. H. *Rev. Sci. Instrum., in press*.
(15) Kiefer, J. H.; Shah, J. N. *J. Chem. Phys.*, **1987**, *91*, 3024.
(16) Krizancic, I.; Haluk, M.; Cho, S. H.; Trass, O. *Rev. Sci. Instrum.* **1979**, *50*, 909.

(17) Kern, R. D.; Singh, H. J.; Zhang, Q. In *Handbook of Shock Waves*; Ben-Dor, G., Igra, O., Lifshitz, A., Eds.; Academic Press: New York, 2001; Vol. 3, Chapter 16.1.

(18) Gaydon, A. G.; Hurle, I. R. *The Shock Tube in High Temperature Chemical Physics*; Chapman and Hall Ltd.: London, 1963.

(19) Moulton, D. McL. Ph.D. Thesis, Harvard University, Boston, MA, 1964.

(20) Dove, J. E.; Moulton, D. McL. *Proc. R. Soc. London A* **1965**, *283*, 216.

(21) Voldner, E. C.; Trass, O. *J. Chem. Phys.* **1980**, *73*, 1601.

(22) Cotter, R. J. In *Time-of-Flight Mass Spectrometry*; Cotter, R. J., Ed.; ACS Symposium Series 549, American Chemical Society: Washington, DC, 1994; p 17.

(23) NIST Mass Spec Data Center, Stein, S. E.; director, Mass Spectra. In *NIST Chemistry WebBook*; Linstrom P. J., Mallard, W. G., Eds.; NIST Standard Reference Database Number 69; National Institute ofStandards and Technology: Gaithersburg MD, 2005; http://webbook.nist.gov.

(24) Kiefer, J. H.; Sidhu, S. S.; Kern, R. D.; Xie, K.; Chen, H.; Harding, L. B. *Combust. Sci. Technol.* **1992**, *82*, 101.

(25) Burcat, A.; Ruscic, B. *Third Millennium Ideal Gas and Condensed Phase Thermochemical Database for Combustion with updates from Active Thermochemical Tables ANL-05/20 and TAE 960*; Technion-IIT, Aerospace Engineering, and Argonne National Laboratory, Chemistry Division, Sept 2005.

(26) Simmi, J. M.; Tschuikow-Roux, E. *J. Chem. Soc., Chem. Commun.* **1970**, *74*, 4075.

(27) Reid, R. C.; Praunsitz, B. E.; Poling, B. E. *The Properties of Liquids and Gases*, 4th ed; McGraw-Hill Book Co.: New York, 1987.